PROCEEDINGS OF SCIENCE

Anisotropic diffusion cannot explain TeV halo observations

Pedro De la Torre Luque,[a,*] **Ottavio Fornieri**[b,c] **and Tim Linden**[a]

[a] *Stockholm University and The Oskar Klein Centre for Cosmoparticle Physics, Alba Nova, 10691 Stockholm, Sweden*

[b] *Gran Sasso Science Institute, Viale Francesco Crispi 7, 67100 L'Aquila, Italy*

[c] *INFN Laboratori Nazionali del Gran Sasso, Via G. Acitelli 22, 67100 Assergi (AQ), Italy*

E-mail: pedro.delatorreluque@fysik.su.se, ottavio.fornieri@gssi.it, linden@fysik.su.se

TeV halos are regions of enhanced photon emissivity surrounding pulsars. While multiple sources have been discovered, a self-consistent explanation of their radial profile and spherically-symmetric morphology remains elusive due to the difficulty in confining high-energy electrons and positrons within ∼20 pc regions of the interstellar medium. One proposed solution utilizes anisotropic diffusion to confine the electron population within a "tube" that is auspiciously oriented along the line of sight. In this work, we show that while such models may explain a unique source such as Geminga, the phase space of such solutions is very small and they are unable to simultaneously explain the size and approximate radial symmetry of the TeV halo population.

27th European Cosmic Ray Symposium (ECRS 2022)
25-29 July 2022
Nijmegen, the Netherlands

*Speaker

PoS(ECRS)109

1. Introduction

TeV halos are a new class of high energy γ-ray sources that are powered by pulsars [1]. The primary observational characteristics of TeV halos include: (1) a hard γ-ray spectrum consistent with inverse-Compton (IC) scattering, (2) a roughly spherically symmetric emission morphology that does not trace Galactic gas, (3) diffusive particle propagation that extends out to ∼10–50 pc [2, 3]. This final observation is noteworthy, because TeV halos are larger than pulsar wind nebulae (PWNe) and remain bright for a longer period than supernova remnants (SNRs), but are more compact than expected for particle propagation in the standard interstellar medium (ISM).

Our understanding of TeV halos hinges on one key question: are TeV halos produced in peculiar regions of the ISM that have *pre-existing* conditions ripe for halo formation? Or, conversely, are TeV halos produced throughout the bulk of the ISM and powered by the natal object which produces a local environment necessary for halo formation? In the former case, only a small fraction of pulsars will produce observable TeV halos. In the latter, TeV halos are expected to surround most energetic pulsars. Observations support the latter case.

Several classes of models have been proposed to explain TeV halos. One popular model focuses on the potential for CRs accelerated by the pulsar or associated SNR [4] to excite a resonant streaming instability that self-confines the CRs near the source [5, 6]. These models potentially explain the evolution of halos, but many complexities of CR turbulence must be solved to make precise predictions. Rectilinear propagation models argue that diffusion is not inhibited, but particle propagation is instead ballistic on small scales, which produces an effective suppression of high-angle emission [7]. However, such models may require an unphysically high efficiency for the pulsar e^+e^- production [8]. Finally, another kind of model argued that the apparent angular size of Geminga and Monogem are consequences of anisotropic diffusion with a maximal diffusion constant similar to the galactic average. In this scenario, the direction of efficient diffusion is oriented along the line-of-sight (LoS) towards Earth, while diffusion is strongly inhibited in the two visible directions perpendicular to the LoS [9]. This model is theoretically motivated by synchrotron polarization measurements which indicate that local diffusion is dominated by flux tubes on scales between 1–100 pc [10, 11]. However, such a model does not predict that many TeV halos would be seen, as observable halos would only be expected from sources that have flux tubes that are fortuitously aligned towards Earth.

Here, we systematically re-examine the class of anisotropic diffusion models. We show that they cannot simultaneously account for the radial size and approximate spherical symmetry of the observed TeV halo population. We note that this conclusion holds for any CR-powered source (hadronic or leptonic), implying more generally that anisotropic diffusion does not dominate the propagation of particles near energetic sources.

2. Anisotropic lepton diffusion around PWN

To study the lepton distribution, $u(\mathbf{r}, t, E_e)$, around pulsars, we can make use of the standard transport equation [12]. The full (general) transport equation is written in terms of a diffusion tensor D_{ij} accounting for the different propagation direction with respect to the orientation of the local magnetic field. With this regards, the diffusion of charged particles depends in fact on

$\mathbf{B}_{\rm tot} = \mathbf{B}_0 + \delta\mathbf{B}$, namely the sum of a large-scale background field ($\mathbf{B}_0$), with a coherence scale between $\sim 1 - 100\,$pc [13], and a small-scale perturbation ($\delta\mathbf{B}$) that depends on the size of the source that is injecting turbulence.

To account for the effect of the magnetic field structure in particle transport, it is useful to decompose the diffusion tensor into directions parallel and perpendicular to the large-scale magnetic field lines. Placing the background magnetic field along the **z**-axis, we exploit the axisymmetric nature of the problem and write $D_{xx} = D_{yy} = D_\perp$, $D_{zz} = D_\parallel$. This allows us to solve the transport equation in cylindrical coordinates (r, z, ϕ), for a cylinder oriented along the **z** axis, such that $D_{zz} = D_\parallel$ and $D_{rr} = D_\perp$, where r is the polar coordinate $\sqrt{x^2 + y^2} = r$. As a consequence, we need to solve the following equation:

$$\frac{\partial u}{\partial t}(r,z,t,E_e) = \frac{1}{r}\frac{\partial}{\partial r}\left(rD_\perp\frac{\partial u}{\partial r}(r,z,t,E_e)\right) + \frac{\partial}{\partial z}\left(D_\parallel\frac{\partial u}{\partial z}(r,z,t,E_e)\right) + \\ + \frac{\partial}{\partial E_e}\left(\frac{\partial E_e}{\partial t}\,u(r,z,t,E_e)\right) + \mathcal{S}(r,z,t,E_e) \tag{1}$$

where, due to the cylindrical symmetry, the gradients involving the azimuthal coordinate ϕ vanish.

Parallel diffusion is the result of the scattering of particles against $\delta\mathbf{B}$, while (mainly) the random walk of the lines themselves (*field-line random walk*) is responsible for perpendicular diffusion. Therefore, if the injected turbulence is strong enough to considerably affect the preferential direction of the background field $\mathbf{B}_0$ on small scales, particle motion tends not to have a privileged direction, and is instead isotropic. Conversely, a weak turbulence does not alter the direction of $\mathbf{B}_0$. The intensity of the injected turbulence is represented by the so-called *Alfvénic Mach number*, defined as $M_A \approx \left(\delta B / B_0\right)\big|_{L_{\rm inj}}$ at the turbulence injection length-scale, $L_{\rm inj}$.

The anisotropic-diffusion explanation for the origin of the TeV halos implies that, whenever the direction of $\mathbf{B}_{\rm tot} \simeq \mathbf{B}_0$ is oriented with our LoS, we observe the halo in only the directions where diffusion is inhibited, and the low-diffusion coefficient becomes a projection effect [9]. Quantitatively, we fix $D_\parallel$ — which is unaffected by the LoS projection — to match cosmic-ray (CR) measurements (*e.g.* the boron-over-carbon ratio) and set the perpendicular diffusion coefficient using the model $D_\perp = D_\parallel M_A^4$ derived by Ref. [14]. TeV halo observations constrain our models to $0 < M_A \leq 1$, which spans from the very anisotropic case ($\delta B \ll B_0$, or $M_A \simeq 0.1$) to the isotropic one ($\delta B = B_0$, or $M_A = 1$). This implies that particle diffusion perpendicular to the local field can be strongly inhibited, depending on the turbulence strength and injection scale.

Equation (1) cannot be solved analytically. In this paper we numerically evolve our system using a Crank-Nicolson scheme [15]. We examine values of M_A spanning from 0.1 to 1 and align the large-scale magnetic field with the **z**-axis. The diffusion equation is evolved on a 2D grid of radius 60 pc and height $[-60\,\text{pc}, +60\,\text{pc}]$ with $(N_r,\, N_z) = (200,\, 200)$ points. Adopting a reference distance to Geminga of $d_{\rm Gem} = 250\,$pc, this corresponds to a window $\Delta\phi \simeq [-13^\circ, +13^\circ]$ and angular resolution $\phi_{\rm res} \simeq 0.1^\circ$.

We assume that the leptons are injected from a point-like pulsar source, noting that the assumed source size does not affect our results. Drawing on pulsar observations, we set the luminosity function to $L(t) = L_0 \times (1 + t/\tau_0)^{-\frac{n+1}{n-1}}$, where L_0 is the luminosity of the source at $t = 0$, n is the braking index and τ_0 is the pulsar spin-down timescale. In our simulations we set $L_0 = 2.8 \times 10^{37}\,\text{erg}\,\text{s}^{-1}$, $\tau_0 = 12\,$kyr and $n = 3$, and normalize our results by imposing that

the total energy released by the pulsar since its birth is $W_e = 1.1 \times 10^{49}$ erg, consistent with previous studies [5, 9, 16, 17]. We convert this spin-down power into electron and positron pairs with an efficiency η, which is fit to data, but cannot exceed 1, yielding an injection spectrum $Q(E_e) = \eta\, Q_0 \left(E_e \,/\, \mathrm{GeV}\right)^{-\alpha} \times e^{-E_e/E_{\rm cut}}$, where $\alpha = 1.6$ [18] and $E_{\rm cut} = 200$ TeV, and Q_0 is a normalization constant. We compute the electron flux from $0.1 - 300$ TeV and the IC-produced γ-ray flux from $0.1 - 200$ TeV. In our setup, we stop the simulation at the age of Geminga, $t_{\rm ch} \sim 342$ kyr.

We parameterize the energy scaling of parallel diffusion as $D_{\parallel} = D_0 \left(E \,/\, E_0\right)^{\delta}$, where D_0 is set at a chosen normalization energy E_0 and δ is derived from the spectral index of the turbulent power spectrum. We fix $D_0 = 3.8 \times 10^{28}\,\mathrm{cm^2\,s^{-1}}$ at $E_0 = 1$ GeV and consider a Kolmogorov spectrum for which $\delta = 0.33$, compatible with standard ISM parameters. Once propagation of particles is computed, leptons interact with their environment to produce bright γ-ray emission, predominantly through inverse-Compton scattering (IC) off the surrounding Interstellar Radiation Field (ISRF) [19]. Full details in the set-up can be found in Ref. [20].

3. Consequences of anisotropic propagation

Using the modelling described above, we produce mock observations for Geminga-like TeV halos for various quantities of the parameters M_A and the inclination angle of the simulation with respect to the LoS, $\psi_{\rm incl}$.

Figure 1 (top) shows the morphology of the γ-ray emissivity as a function of r and z at 20 TeV. In Figure 1 (bottom), we show the *observed* extension of the simulated halo as a function of the angle $\psi_{\rm incl}$, which corresponds to rotations of our simulated cylinder with respect to our LoS along the r-axis, and compare our results to the 68% and 82% of the flux contained in the Geminga TeV halo as reported by Ref. [2]. We note that rotations around the **z**-axis do not change the morphology of the halo with respect to our LoS due to the cylindrical symmetry of the system, while rotations around the **r**-axis change the morphology that is projected on the plane-of-the-sky (*c.f.* Figure 2 of Ref. [9]).

Figure 1 demonstrates that, if anisotropic diffusion produces TeV halos, we should detect a variety of both highly extended and asymmetric objects (as seen at different inclination angles, $\psi_{\rm incl}$). This is in tension with the fact that observed TeV halos have similar sizes and approximate spherical symmetry. The model is constrained from two directions: (i) for values of $M_A \leq 0.5$, the asymmetry of each TeV halo becomes pronounced and observations would show “ovals" or "strings" in the TeV sky, while spherically symmetric halos would be observed only when $\psi_{\rm incl} \sim 0°$. (ii) for values of $M_A \geq 0.5$ the halo appears roughly spherically symmetric, but the lack of inhibited diffusion makes the halo too large to explain observed systems. Notably, we see that for $M_A \geq 0.5$ there is no value of $\psi_{\rm incl}$ for which the containment angle along the **z**-axis is consistent with HAWC observations of Geminga.

We can formalize the excluded $\psi_{\rm incl}$ angles based on the morphology and symmetry of simulated TeV halos by imposing two conditions: (i) that the emission should not be very asymmetric (*i.e.* the extension of the halo in any direction should not be much larger than the extension in the perpendicular one). (ii) the size of the emission should not be much larger than 5.5° (*i.e.* 24 pc, given the distance from Geminga), to be consistent with the size of Geminga reported in Ref. [2],

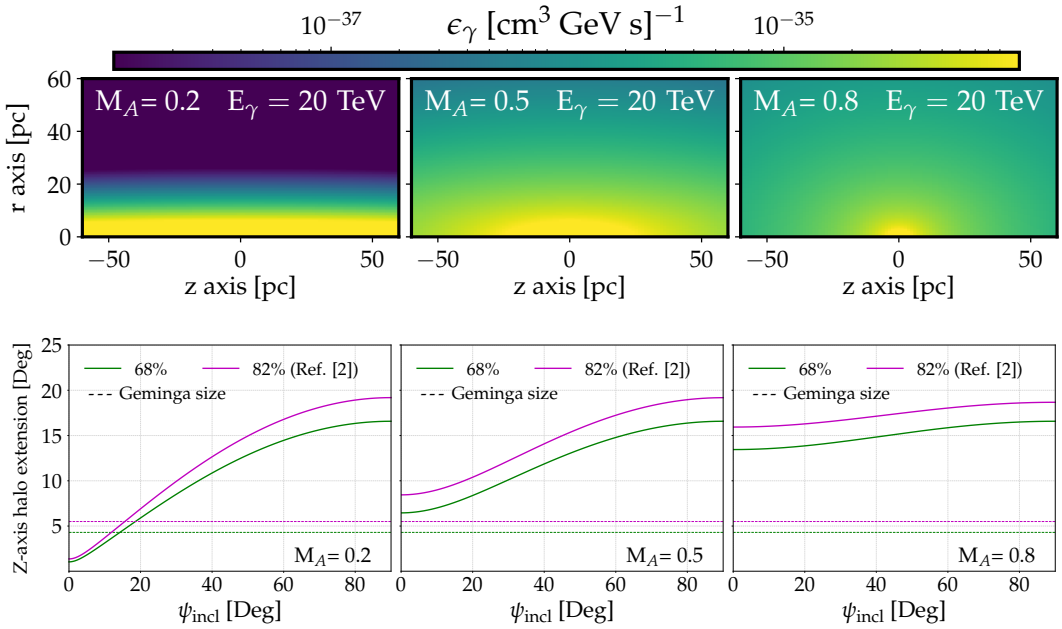

Figure 1: Top panels: γ-ray emissivity maps for different levels of anisotropic emission ($M_A = 0.2$, $M_A = 0.5$ and $M_A = 0.8$) at $E_\gamma = 20$ TeV. **Bottom panels:** TeV halo extension projected on the plane-of-sky, along the Z-axis for different inclination angles ($\psi_{\rm incl}$), compared to the Geminga's TeV halo size for $\sim 68\%$ and $\sim 82\%$ of the flux contained around the source (green and magenta dashed lines, respectively). A simulation with a larger window (120 pc) has been used to correctly compute the total extension of the halo.

which corresponds to $\sim 82\%$ of the flux contained around the source. We additionally calculate the size the halo at $\sim 68\%$ ($\sim 1\sigma$) containment, which is 4.3° (~ 19 pc) for Geminga.

To quantify the first condition (hereafter, the *symmetry condition*) we impose that the projected extension of the halo in one direction must not be more than 100% larger than in the other direction ($Z/R < 2$), which is a very conservative choice. The second condition (hereafter, the *size condition*, see bottom panels of Figure 1) imposes that the extension of the halo projected on the plane-of-sky along Z is within the size uncertainty reported by HAWC, which is $5.5 \pm 0.7°$ ($\sim 24 \pm 3$ pc). While the first condition only depends on the ratio $D_\perp / D_\parallel = M_A^4$, the second depends on both such ratio and the normalization of $D_\parallel$, which is fixed to the diffusion coefficient obtained from analyses of CR secondary-to-primary ratios. Since the normalization of the $D_\parallel$ in the Galaxy is uncertain by at least $\sim 30\%$, mainly due to cross sections uncertainties [21–23], we have also tested other values of the normalization of $D_\parallel$ around $D_0 = 3.8 \times 10^{28}$ cm^2 s^{-1}, as we discuss below.

In Figure 2, we show the constraint on the TeV halo population in the parameter space of M_A and $\psi_{\rm incl}$. Only a very reduced space of inclination angles ($\psi_{\rm incl} < 5°$) is able to simultaneously account for the radial size and measured symmetry of a typical TeV halo. This means that, unless there is a reason to believe that all existing TeV halos are aligned with our LoS, the anisotropic model is not able to explain the observation of multiple symmetric TeV halos and the lack of observed asymmetric ones.

The relatively simple *symmetry* and *size* conditions already rule out the vast majority of the $M_A / \psi_{\rm incl}$ parameter space. Additionally, the emission profile is expected to show clear signatures of

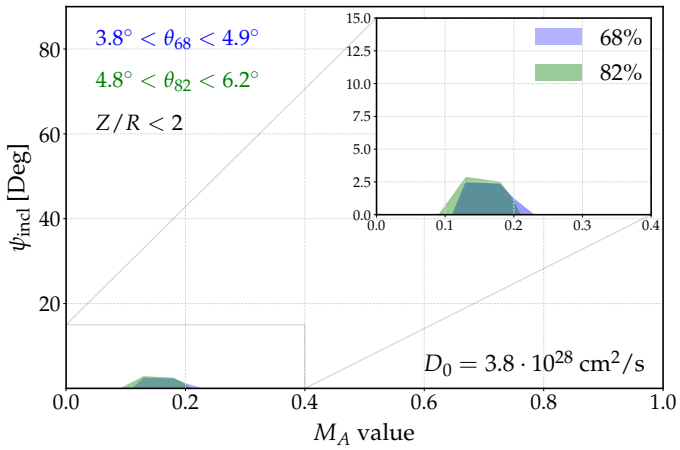

Figure 2: The parameter space of inclination angles ($\psi_{\rm incl}$) and asymmetric diffusion parameters which produce TeV halos that fulfill the symmetry ($Z/R < 2$) and size ($\theta_c \sim \theta_{\rm Geminga} \pm 1\sigma$) conditions at both 68% and 82% containment.

anisotropic diffusion when performed following independently perpendicular axes (i.e. the surface brightness along the different axes is expected to be different). These signatures would be detectable, although no collaboration reported this kind of differences yet. In Figure 3 we show the emission profiles in both the **r** (perpendicular to the magnetic field) and **z** (parallel to the field) directions for values of $M_A = 0.1$, $M_A = 0.3$ and $M_A = 1$. Given the anisotropic structure of the predicted halos, the profile is computed along the Z and R axes separately. To have a qualitative comparison, HAWC's surface brightness [19] is also shown, although their points are obtained averaging the emission in rings around the center of the object. As discussed, in the case of an asymmetric halo in the $\psi_{\rm incl} = 90°$ case, observations would detect a profile that is starkly different in each direction (at least for $M_A \leq 0.5$). This remains valid for angles $\psi_{\rm incl} > 0°$.

4. Conclusions

In this work, we have demonstrated that one of the more popular models, where anisotropies in local diffusion explain the TeV halo morphology, is inconsistent with TeV halo observations. Specifically, we have explored and analyzed different morphological signatures of anisotropic diffusion that are predicted by this model but are not observed in detected TeV halos.

We have analyzed the morphology of anisotropic TeV halos as a function of two key parameters: M_A, which controls the ratio of the diffusion coefficients perpendicular to and along the background magnetic field, and $\psi_{\rm incl}$, which controls the angle between the magnetic field and the observer's LoS. Our results constrain anisotropic TeV halo models in three ways: (1) we constrain M_A to be smaller than ~ 0.5 to prevent the TeV Halos from becoming too large compared to current measurements, (2) we constrain $\psi_{\rm incl}$ to be less than $\sim 5°$ in order to prevent observed TeV halos from having a significant visual asymmetry that would appear oblong or "spaghetti shaped" on the sky, (3) we show that the expected surface brightness along different axes is significantly different for asymmetric objects, which could lead to easily discard values of M_A smaller than ~ 0.3. In this

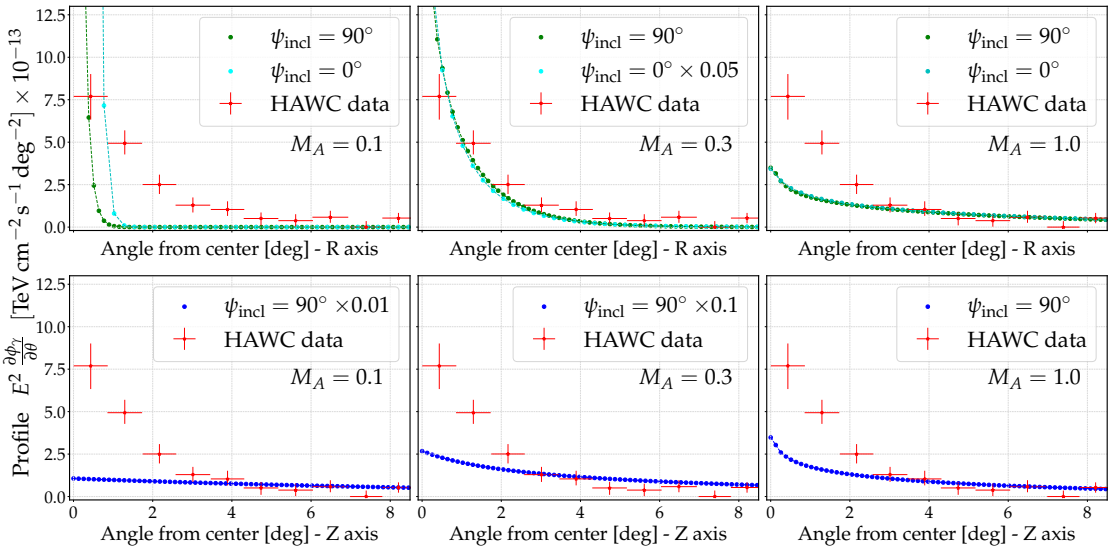

Figure 3: Gamma-ray surface brightness for different values of M_A ($M_A = 0.1, 0.3, 1$) at $\psi_{\rm incl} = 90°$ and $\psi_{\rm incl} = 0°$, compared to the HAWC surface brightness. **Top panels**: gamma-ray emission profile along R-axis. **Bottom panels**: gamma-ray emission along Z-axis. The emission is integrated for gamma-ray energies from 5 to 50 TeV. For each M_A, the intensity is scaled by the number shown in the legend. There is no $\psi_{\rm incl} = 0°$ line in the Z-case: such axis would be aligned with our LoS and thus the extension is not observed.

context, we stress that it would be crucial to experimentally measure the profile along the different axes, since such a test would be able to unequivocally detect signatures of anisotropic diffusion.

To be precise, our analysis indicates that anisotropic diffusion cannot explain the observation of several TeV halos in any scenario where the diffusion coefficient in the uninhibited direction is compatible with best-fit values from galactic secondary-to-primary ratios. Our models leave open the possibility that the diffusion coefficient surrounding TeV halos is mildly anisotropic. However the diffusion coefficient in every direction must be significantly inhibited compared to the average diffusion coefficient of the Milky Way. Although our analysis is based on the anisotropic-diffusion model put forward in Yan and Lazarian [14], our conclusions remain valid for any anisotropic model where the scalings of the perpendicular and parallel diffusion coefficients are similar — namely $\delta_\parallel \simeq \delta_\perp$, given the typical parameterization $D_{\parallel,\perp} \propto E^{\delta_\parallel, \delta_\perp}$ — which is supported by numerical simulations [24].

Finally, we stress that observations of suppressed and spherically symmetric diffusion provide further credence in favor of models where the diffusivity is reduced not due to a geometrical effect, but rather *intrinsically* inhibited/subdominant due to subtle mechanisms, either generated by the compact object or pre-existing in the region.

References

[1] T. Linden *et al.*, Phys. Rev. D **96**, 103016 (2017), arXiv:1703.09704 [astro-ph.HE] .

[2] A. U. Abeysekara *et al.*, Astrophys. J. **843**, 40 (2017), arXiv:1702.02992 [astro-ph.HE] .

[3] R. López-Coto *et al.*, Nature Astronomy **6**, 199 (2022).

[4] K. Fang *et al.*, MNRAS **488**, 4074 (2019), arXiv:1903.06421 .

[5] C. Evoli, T. Linden, and G. Morlino, PRD **98**, 063017 (2018).

[6] P. Mukhopadhyay and T. Linden, (2021), arXiv:2111.01143 .

[7] S. Recchia *et al.*, Phys. Rev. D **104**, 123017 (2021), arXiv:2106.02275 [astro-ph.HE] .

[8] L.-Z. Bao *et al.*, (2021), arXiv:2107.07395 .

[9] R.-Y. Liu, H. Yan, and H. Zhang, PRL **123**, 221103 (2019).

[10] M. Haverkorn *et al.*, Astrophys. J. **680**, 362 (2008), arXiv:0802.2740 [astro-ph] .

[11] M. Iacobelli *et al.*, Astron. Astrophys. **558**, A72 (2013), arXiv:1308.2804 .

[12] Ginzburg and Syrovatskii, *The Origin of Cosmic Rays* (1964).

[13] A. W. Strong, I. V. Moskalenko, and V. S. Ptuskin, Ann. Rev. Nucl. Part. Sci. **57**, 285 (2007), arXiv:astro-ph/0701517 .

[14] H. Yan and A. Lazarian, **673**, 942 (2008).

[15] J. Crank and P. Nicolson, Mathematical Proceedings of the Cambridge Philosophical Society **43**, 50–67 (1947).

[16] S. Recchia *et al.*, (2021), arXiv:2106.02275 [astro-ph.HE] .

[17] M. Di Mauro *et al.*, Phys. Rev. D **100**, 123015 (2019).

[18] D. Hooper *et al.*, Phys. Rev. D **96**, 103013 (2017), arXiv:1702.08436 .

[19] A. U. Abeysekara *et al.* (HAWC), Science **358**, 911 (2017), arXiv:1711.06223 [astro-ph.HE] .

[20] P. De La Torre Luque, O. Fornieri, and T. Linden, (2022), arXiv:2205.08544 [astro-ph.HE] .

[21] P. De La Torre Luque *et al.*, JCAP **03**, 099 (2021), arXiv:2101.01547 .

[22] P. D. L. T. Luque, JCAP **11**, 018 (2021), arXiv:2107.06863 .

[23] M. Korsmeier and A. Cuoco, Phys. Rev. D **103**, 103016 (2021), arXiv:2103.09824 [astro-ph.HE] .

[24] G. Giacinti, M. Kachelriess, and D. V. Semikoz, JCAP **07**, 051 (2018), arXiv:1710.08205 [astro-ph.HE] .